New Astronomy 82 (2021) 101447

Contents lists available at ScienceDirect

New Astronomy

journal homepage: www.elsevier.com/locate/newast

Photoionization features of the ground and excited levels of Cl II and benchmarking with experiment

Sultana N. Nahar*

Department of Astronomy, The Ohio State University, Columbus, OH 43210, United States

ARTICLE INFO

Keywords:
Photoionization of Cl II
Breit-Pauli R-matrix method
Rydberg and seaton resonances
Benchmarking with experiment
32.10-f
95.30.Ky
32.80-t

ABSTRACT

This report presents i) various characteristic features in photoionization cross sections (σ_{PI}) of Cl II + hν $\rightarrow$ Cl III + e for many fine structure levels of Cl II, 392 in total with $n \leq 10$ and $l \leq 9$, ii) comparison of features with those observed in an experiment carried out at the Advanced Light Source at Lawrence Berkeley National Lab, and iii) partial photoionization cross sections of the ground level for ionization leaving the core ion in to various excited levels for applications in plasma modeling. The features correspond to resonant structures, the shape of the background, and their interference effect in σ_{PI} of this near neutral ion Cl II with 16 electrons. σ_{PI} for the 5 levels of the ground configuration $3s^23p^4(^3P_{0,1,2}, {}^1D_2, {}^1S_0)$ of Cl II show regions of narrow Rydberg resonances at and near threshold energies, and resonant structures at higher energies in contrast to typical smooth decrease in the background. Various other features in σ_{PI} of levels of excited equivalent electron states and broad Seaton resonances in single valence electron excited levels are illustrated with examples. Comparison of calculated σ_{PI} of the 15 lowest levels with the combined features of the measured photoionization spectrum shows excellent agreement by reproducing and thus identifying them to the levels that they belong to. The calculations were carried out in relativistic Breit-Pauli R-matrix (BPRM) method using a close coupling wave function expansion of 45 levels up to 4s of the core ion Cl III. These levels were optimized using a set of 12 configurations going up to orbital 5s, $3s^23p^3$, $3s3p^4$, $3p^5$, $3s^23p^23d$, $3s^23p^24s$, $3s^23p^24p$, $3s^23p^24d$, $3s^23p^24f$, $3s^23p^25s$, $3s3p^33d$, $3s^23p3d^2$, $3p^43d$ producing 283 levels of Cl III. The autoionizing resonances are delineated with a fine energy mesh to observe the fine structure effects. The present results will provide high precision parameters for various applications involving this less studied ion.

1. Introduction

Chlorine is used in variety of applications in our daily life. It exists in astrophysical objects, such as, in low ionization stage in planetary nebula, for example NGC2818 (Dufour, 1984), Jupiter moon Io (e.g. Fegley and Zolotov (2000)), etc and provides physical and chemical information of the objects. Photoionization of Cl II produces Cl III which is commonly observed in the emission spectra of relatively cooler astrophysical plasmas. As an element existing both on the earth and in space, it is important to study the features to help in its identification in astrophysical and laboratory plasmas and modeling for various applications. However, there is a lack of study of its radiative properties. Due to its low abundance, the study under the Opacity Project (OP) (Team, 1996) did not include chlorine.

The first reported study on detailed photoionization cross section of Cl II was from a high resolution experiment carried out at the Advanced Light Source (ALS) at Lawrence Berkeley National Lab (LBNL) by Hernandez et al (Hernandex, 2015) who considered the photon energy range of 19.5 - 28.0 eV. Following this McLaughlin (McLaughin, 2017) reproduced most of the features theoretically by calculating photoionization cross sections (σ_{PI}) of the 5 levels of the ground configuration. He used Dirac-Coulomb R-matrix method and computed the cross sections in the same energy range as that of the experiment. In contrast to these existing studies, the present work reports photoionization cross sections of the ground and many excited levels with $n \leq 10$ and $l \leq 9$ needed for complete astrophysical modeling for all practical applications, presents features of excited levels with Rydberg and Seaton resonances, presents partial cross sections for photoionization into various excited levels of the ion core not studied before but are needed for various applications, and presents comparison with the existing experiment with very good agreement. The present work is carried out under the Iron Project Hummer et al., a follow-up of the Opacity Project

* Corresponding author.
E-mail address: nahar.1@osu.edu.
URL: http://www.astronomy.ohio-state.edu/pl2X-sim-nahar.

https://doi.org/10.1016/j.newast.2020.101447
Received 8 February 2020; Received in revised form 8 July 2020; Accepted 10 July 2020
Available online 11 July 2020

(Team, 1996), that aims in solving astrophysical problems using accurate parameters of the atomic processes in the plasmas.

2. Theory

Photoionization process can be direct as,

$$h\nu + X^{+} \rightarrow e + X^{2+}. \quad (1)$$

or indirect when an intermediate doubly excited state, known as an autoionization state, is formed before ionization.

$$h\nu + X^{+} \leftrightharpoons (X^{+})^{**} \leftrightharpoons e + X^{2+} \quad (2)$$

This autoionizing state forms when the photon energy matches that of a Rydberg state, $S_iL_iJ_i\pi_i\nu_l\ell$ where $S_iL_iJ_i\pi_i$ is an excited core ion state, ν_l is the effective quantum number of the Rydberg series converging on to the excited core ion state. The Rydberg state lies above the ionization threshold but below an excited core ion state, Formation of an autoionizing state introduces a resonance in photoionization and is the reason for features and structures in the process.

The resonances can be generated naturally in an ab initio theoretical calculation by including the core ion excitations in the wave function expansion, as considered in the close coupling (CC) approximation. In CC approximation, the atomic system is represented by a (N+1) number of electrons where the core ion is an N-electrons system interacting with the (N+1)th electron. The (N+1)th electron can be bound or in the continuum depending on its negative or positive energy (E). The total wave function, Ψ_E, in a symmetry $SL\pi$ of the system is expressed by an expansion as (e.g. Pradhan and Nahar, 2011)

$$\Psi_E(e + ion) = A\sum_i \chi_i(ion)\theta_i + \sum_j c_j\Phi_j, \quad (3)$$

where χ_i is the eigenfunction representing ground and various excited levels of the core ion and the sum is over the number of levels considered. The core ion is coupled with the (N+1)th electron function, θ_i, with kinetic energy k_i^2 in a channel labeled as $S_iL_i(J_i)\pi_ik_i^2\ell_i[SL(J)\pi]$. A is the antisymmetrization operator. In the second sum, the Φ_js are bound channel functions of the (N+1)-electrons system that provides the orthogonality between the continuum and the bound electron orbitals and account for short range correlation. Substitution of $\Psi_E(e + ion)$ in the Schrodinger equation

$$H_{N+1}^{BP}\Psi_E = E\Psi_E \quad (4)$$

introduces a set of coupled equations that are solved using the R-matrix approach. The details of the R-matrix method in the CC approximation can be found in, e.g. Burke and Robb (1975), Seaton (1987), Berrington et al. (1987), Berrington et al. (1995), Pradhan and Nahar (2011). The relativistic effects are included through Breit-Pauli approximation (e.g. Pradhan and Nahar, 2011) where the Hamiltonian is given by

$$H_{N+1}^{\rm BP} = \sum_{i=1}^{N+1}\left\{-\nabla_i^2 - \frac{2Z}{r_i} + \sum_{j>i}^{N+1}\frac{2}{r_{ij}}\right\} + H_{N+1}^{\rm mass} + H_{N+1}^{\rm Dar} + H_{N+1}^{\rm so}, \quad (5)$$

in Rydberg unit. The relativistic correction terms are mass correction, $H^{\rm mass} = -\frac{\alpha^2}{4}\sum_i p_i^4$, Darwin, $H^{\rm Dar} = \frac{Z\alpha^2}{4}\sum_i \nabla^2(\frac{1}{r_i})$, and spin-orbit interaction, $H^{\rm so} = Z\alpha^2\sum_i \frac{1}{r_i^3}\mathbf{l_i}.\,\mathbf{s_i}$. The R-matrix Breit-Pauli (BPRM) approximation under the Iron Project Hummer et al. includes all these terms and part of two-body interaction terms, such as the ones without the momentum operators (Pradhan and Nahar, 2011). In BPRM method the set of $SL\pi$ is recoupled to $J\pi$ levels of (e + ion) system in intermediate coupling which is followed by diagonalization of the Hamiltonian.

For an electron with positive energies (E > 0) the solution is a continuum wave function, Ψ_F and with negative energy (E ≤ 0) it is a bound state, Ψ_B. The complex resonant structures in photoionization are produced from couplings between continuum channels that are open ($k_i^2 > 0$), and bound channels that are closed ($k_i^2 < 0$), at electron energies k_i^2 of autoionizing Rydberg states, $S_iL_iJ_i\pi_i\nu\ell$ belonging to excited core threshold $S_iL_iJ_i\pi_i$.

The photoionization cross section (σ_{PI}) is given by (e.g. Pradhan and Nahar, 2011)

$$\sigma_{PI} = \frac{4\pi^2}{3c}\frac{1}{g_i}\omega\mathbf{S}, \quad (6)$$

where g_i is the statistical weight factor of the bound state, ω is the incident photon energy and $\mathbf{S}$ is the generalized line strength

$$\mathbf{S} = |<\Psi_f||\mathbf{D}_L||\Psi_i>|^2 = \left|\left\langle\psi_f|\sum_{j=1}^{N+1} r_j|\psi_i\right\rangle\right|^2, \quad (7)$$

whereΨ_i and Ψ_f are the initial and final state wave functions, and $\mathbf{D}_L$ is the dipole operator in length form.

3. Computations

BPRM computations are carried out in a number of stages using the R-matrix package of codes (Berrington et al., 1995; Nahar and Pradhan, 1994; Zhang et al., 1999). They are initiated with the wave function of the core ion as the initial input, such as Cl III in the present case. The wave function expansion of the core ion, Cl III, was obtained from atomic structure calculations using program SUPERSTRUCTURE (SS) (Eissner et al., 1974; Nahar et al., 2003). SS uses Thomas-Fermi-Dirac-Amaldi potential and includes relativistic contributions in Breit-Pauli approximation. Table 1 presents the ground and 44 excited fine structure levels of Cl III included in the wave function expansion of Cl II. They were obtained by optimization of a set of 12 configurations of Cl III with orbitals up to 5s, $3s^23p^3$, $3s3p^4$, $3p^5$, $3s^23p^23d$, $3s^23p^24s$, $3s^23p^24p$, $3s^23p^24d$, $3s^23p^24f$, $3s^23p^25s$, $3s3p^33d$, $3s^23p3d^2$, $3p^43d$. The Thomas-Fermi scaling parameters for the orbitals are 1.2(1s), 1.2(2s), 1.1(2p), 1.25(3s), 1.07(3p), 1.05(3d), 1.2(4s), 1.02(4p), 1.4(4d), 1.0(4f), 1.0(5s). The computation resulted in 283 fine structure levels for Cl III out of which the lowest 45 levels were selected for the R-matrix calculations. The calculated energies from SS are compared with observed values (available at NIST website energies which listed them from the compilation by Martin et al.). Comparison shows agreement between SS and observed values within a few percent mostly. For accurate energy positions of the resonances in σ_{PI} the calculated energies of the core ion Cl III were replaced by the available observed energies during diagonalization of the (N+1)-electron Hamiltonian. As Table 1 shows, not all calculated energies have been observed experimentally.

The wave function of Cl II included $0 \le \ell \le 10$ partial waves for the interacting electron and 18 continuum functions for the R-matrix basis sets. The R-matrix boundary was chosen to be large, 15 a_o, such that the bound orbitals are accommodated inside and amplitudes are near zero at the boundary. The second term of the wave function, which represents the bound state correlation functions, included 32 $(N+1)$-particle configurations with occupancy in the orbitals from minimum to a maximum number as given within parentheses of the orbitals, 1s(2-2), 2s(2-2), 2p (6-6), 3s(0-2), 3p(0-6), 3d(0-3), 4s(0-2), 4p(0-2), 4d(0-1), 4f (0-1), 5s(0-1).

Photoionization cross sections are obtained with consideration of radiation damping for all bound levels using the BPRM codes (Berrington et al., 1995; Zhang et al., 1999). The narrow resonances of photoionization were delineated with a very fine energy mesh.

4. Results and discussions

Detail study of photoionization cross sections (σ_{PI}) of the S-like chlorine ion, Cl II, is reported. A total of 392 bound levels of Cl II with $n \le 10$, $0 \le l \le 9$, $0 \le J \le 10$ of even and odd parities were found. Photoionization cross sections have been obtained for of all these levels. Examples of σ_{PI} illustrating important characteristic features are

Table 1
Levels and energies (E_t) of core ion Cl III included in the wave function expansion of Cl II. Calculated energies from SUPERSTRUCTURE (SS) are compared with those in the NIST table energies.

	Level	J_t	E_t(Ry) NIST	E_t(Ry) SS
1	$3s^23p^3(^4S^o)$	3/2	0.0	0.0
2	$3s^23p^3(^2D^o)$	3/2	0.16450612	0.19339
3	$3s^23p^3(^2D^o)$	5/2	0.16510728	0.19388
4	$3s^23p^3(^2P^o)$	1/2	0.27168443	0.29100
5	$3s^23p^3(^2P^o)$	3/2	0.27252762	0.29149
6	$3s3p4(^4P)$	5/2	0.89778340	0.86048
7	$3s3p^4(^4P)$	3/2	0.90335178	0.86514
8	$3s3p^4(^4P)$	1/2	0.90648490	0.86785
9	$3s3p^4(^2D)$	3/2	1.11294558	1.1049
10	$3s3p^4(^2D)$	5/2	1.11338426	1.1050
11	$3s^23p^23d(^2P)$	3/2		1.2784
12	$3s^23p^23d(^2P)$	1/2		1.2838
13	$3s3p^4(^2S)$	1/2		1.3696
14	$3s^23p^23d(^4F)$	3/2	1.33520416	1.3790
15	$3s^23p^23d(^4F)$	5/2	1.33725697	1.3807
16	$3s^23p^23d(^4F)$	7/2	1.34019653	1.3831
17	$3s^23p^23d(^4F)$	9/2	1.34406914	1.3863
18	$3s^23p^23d(^4D)$	5/2	1.38372621	1.4334
19	$3s^23p^23d(^4D)$	3/2	1.38401472	1.4326
20	$3s^23p^23d(^4D)$	1/2	1.38462062	1.4321
21	$3s^23p^23d(^4D)$	7/2	1.38468523	1.4344
22	$3s^23p^23d(^2F)$	5/2		1.4490
23	$3s^23p^23d(^2F)$	7/2		1.4543
24	$3s^23p^23d(^2G)$	7/2		1.6044
25	$3s^23p^23d(^2G)$	9/2		1.6053
26	$3s^23p^24s(^4P)$	1/2	1.58319236	1.6371
27	$3s^23p^24s(^4P)$	3/2	1.58645233	1.6401
28	$3s^23p^24s(^4P)$	5/2	1.59117944	1.6451
29	$3s^23p^24s(^2P)$	1/2	1.62541920	1.6878
30	$3s^23p^24s(^2P)$	3/2	1.63185329	1.6927
31	$3s^23p^23d(^4P)$	5/2	1.63566939	1.7248
32	$3s^23p^23d(^4P)$	3/2	1.63720198	1.7274
33	$3s^23p^23d(^4P)$	1/2	1.63828356	1.7289
34	$3s^23p^23d(^2D)$	3/2	1.65919623	1.7004
35	$3s^23p^23d(^2D)$	5/2	1.66800061	1.8025
36	$3s^23p^23d(^2P)$	3/2	1.69347755	1.8925
37	$3s^23p^23d(^2P)$	1/2	1.69695849	1.8895
38	$3s^23p^24s(^2D)$	5/2	1.71673171	1.7062
39	$3s^23p^24s(^2D)$	3/2	1.71726016	1.8020
40	$3s^23p^23d(^2D)$	5/2	1.77659522	1.8795
41	$3s^23p^23d(^2D)$	3/2	1.77941076	1.8824
42	$3s^23p^23d(^2F)$	5/2	1.78733386	1.9015
43	$3s^23p^23d(^2F)$	7/2	1.78748094	1.9017
44	$3s3p^4(^2P)$	1/2	1.81192012	1.7821
45	$3s3p^4(^2P)$	3/2	1.81327371	1.7774

discussed below the table of Cl II energies.

4.1. Energy levels of Cl II

All 392 energies of Cl II from BPRM calculations have been identified with spectroscopic designation. The BPRM codes calculate the Eigen values of the Hamiltonian as energies which can be obtained by scanning through the poles of the Hamiltonian matrix using a smaller energy mesh. Fine energy meshes of effective quantum number of 0.001 and 0.0005 were used to obtain the 392 energy levels of Cl II. These levels were designated with spectroscopic notation following a theoretical algorithm described in Nahar and Pradhan (2000), Nahar (2014) which is based on the quantum defect analysis, percentage of channels contribution, and angular momenta algebra. Even with fine energy mesh used here, some observed energy levels are found to be missing in the calculated set. A sample set of identified energies and comparison with measured values by Radziemski and Kaufman (1974) listed at NIST website energies are given in Table 2. The complete table will be available electronically from database NORAD-Atomic-Data website. Out of 237 observed energies that were compared with the calculated

Table 2
Comparison between the present calculated BPRM and observed energies of Cl II by Radziemski and Kauffman (Radziemski and Kaufman, 1974). I_J is the calculated level index for its position in its $J\pi$ symmetry. Negative sign for energies is omitted for convenience .

Level		$J : I_J$	E(Ry,BPRM)	E(Ry,NIST)
$3s^23p^4$	^3P	2 :1	1.92331E+00	1.75027E+00
$3s^23p^4$	^3P	1 :1	1.91824E+00	1.74393E+00
$3s^23p^4$	^3P	0 :1	1.91591E+00	1.74119E+00
$3s^23p^4$	^1D	2 :2	1.80110E+00	1.64408E+00
$3s^23p^4$	^1S	0 :2	1.57810E+00	1.49623E+00
$3s3p^5$	$^3P^o$	2 :1	9.70720E−01	8.99443E−01
$3s3p^5$	$^3P^o$	1 :1	9.66112E−01	8.93681E−01
$3s3p^5$	$^3P^o$	0 :1	9.63752E−01	8.90637E−01
$3s^23p^3(^4S^o)4s$	$^5S^o$	2 :3	7.72628E−01	7.67199E−01
$3s^23p^3(^4S^o)3d$	$^5D^o$	4 :1	7.77328E−01	7.45172E−01
$3s^23p^3(^4S^o)3d$	$^5D^o$	3 :1	7.77516E−01	7.45164E−01
$3s^23p^3(^4S^o)3d$	$^5D^o$	2 :2	7.77656E−01	7.45138E−01
$3s^23p^3(^4S^o)3d$	$^5D^o$	1 :3	7.32228E−01	7.45114E−01
$3s^23p^3(^4S^o)3d$	$^5D^o$	0 :2	7.77796E−01	7.45102E−01
$3s^23p^3(^4S^o)4s$	$^3S^o$	1 :4	7.17728E−01	7.24098E−01
$3s^23p^3(^2D^o)3d$	$^1P^o$	1 :5	6.78968E−01	6.96319E−01
$3s^23p^3(^4S^o)3d$	$^3D^o$	3 :2	6.79604E−01	6.58470E−01
$3s^23p^3(^4S^o)3d$	$^3D^o$	2 :4	6.79356E−01	6.58570E−01
$3s^23p^3(^4S^o)3d$	$^3D^o$	1 :6	5.79924E−01	6.58178E−01
$3s^23p^3(^2D^o)3d$	$^1S^o$	0 :3	6.19784E−01	6.08946E−01
$3s^23p^3(^2D^o)3d$	$^3F^o$	4 :2	6.10804E−01	5.97899E−01
$3s^23p^3(^2D^o)3d$	$^3F^o$	3 :3	6.12732E−01	6.00062E−01
$3s^23p^3(^2D^o)3d$	$^3F^o$	2 :5	6.14244E−01	6.01768E−01
$3s^23p^3(^2D^o)4s$	$^3D^o$	3 :4	5.79608E−01	5.94926E−01
$3s^23p^3(^2D^o)4s$	$^3D^o$	2 :6	5.79832E−01	5.95285E−01
$3s^23p^3(^2D^o)4s$	$^3D^o$	1 :7	4.67060E−01	5.95452E−01
$3s^23p^3(^4S^o)4p$	^5P	3 :1	5.54112E−01	5.77189E−01
$3s^23p^3(^4S^o)4p$	^5P	2 :3	5.54668E−01	5.77802E−01
$3s^23p^3(^4S^o)4p$	^5P	1 :2	5.55020E−01	5.78172E−01
$3s^23p^3(^2D^o)4s$	$^1D^o$	2 :7	5.54360E−01	5.74126E−01
$3s^23p^3(^4S^o)4p$	^3P	2 :4	5.19464E−01	5.49506E−01
$3s^23p^3(^4S^o)4p$	^3P	1 :3	5.19400E−01	5.49620E−01
$3s^23p^3(^4S^o)4p$	^3P	0 :3	5.19268E−01	5.49499E−01
$3s^23p^3(^2D^o)3d$	$^3G^o$	5 :1	5.54024E−01	5.45638E−01
$3s^23p^3(^2D^o)3d$	$^3G^o$	4 :3	5.54556E−01	5.45802E−01
$3s^23p^3(^2D^o)3d$	$^3G^o$	3 :5	5.54968E−01	5.45902E−01
$3s^23p^3(^2D^o)3d$	$^1G^o$	4 :4	5.32312E−01	5.25589E−01
$3s^23p^3(^2P^o)4s$	$^3P^o$	2 :8	4.82972E−01	4.93821E−01
$3s^23p^3(^2P^o)4s$	$^3P^o$	1 :8	4.59352E−01	4.94488E−01
$3s^23p^3(^2P^o)4s$	$^3P^o$	0 :4	4.59884E−01	4.94802E−01

levels, the percent discrepancy is less than 5% for 111 levels. Some show large discrepancy, such as the three levels of the ground state ^3P for which the discrepancy is 10%. They indicate the agreement between theory and measurement is fair to good in general. Uncertainties in energies of near neutral ions is common because of larger perturbation effect from electron-electron correlation compared to strong nuclear attraction in highly charged ions. The cause for uncertainties may also come from other reasons, such as, matching of identifications of levels by Radziemski and Kaufman (1974) and the present work, difference in mixing coefficients between the two identifications and number of dominant configurations contributing to the levels Nahar and Pradhan, 2000.

4.2. Photoionization of the 5 levels of the ground configuration

Fig. 1 presents photoionization cross sections (σ_{PI}) of the 5 levels of the ground configuration $3s^23p^2$ of Cl II, the ground level $^3P_0$ and four excited metastable levels, $^3P_{1,2}$, $^1D_2$, $^1S_0$. The present work shows region of narrow resonances at and near threshold energies of each of these levels. σ_{PI} below the first excitation thresholds of $3s^23p^3(^2D^o_{3/2,5/2})$ (pointed by a red arrow at the averaged $^2D^o$ position) of the core ion has near zero background but relatively high peak resonances. In this region, the possible continuum channels are $3s^23p^3(^4S^o_{3/2})(\varepsilon d, \varepsilon s)$ giving $^3D^o_{1,2,3}$ and $^3S^o_1$ levels, but not $^3P^o_{0,1,2}$. These couple with the Rydberg fine structure levels $3s^23p^3(^2D^o_{3/2,5/2})[\nu d(^3S^o_1, ^3D^o_{1,2,3}),\ \nu s(^3S^o_1)]$ belonging to

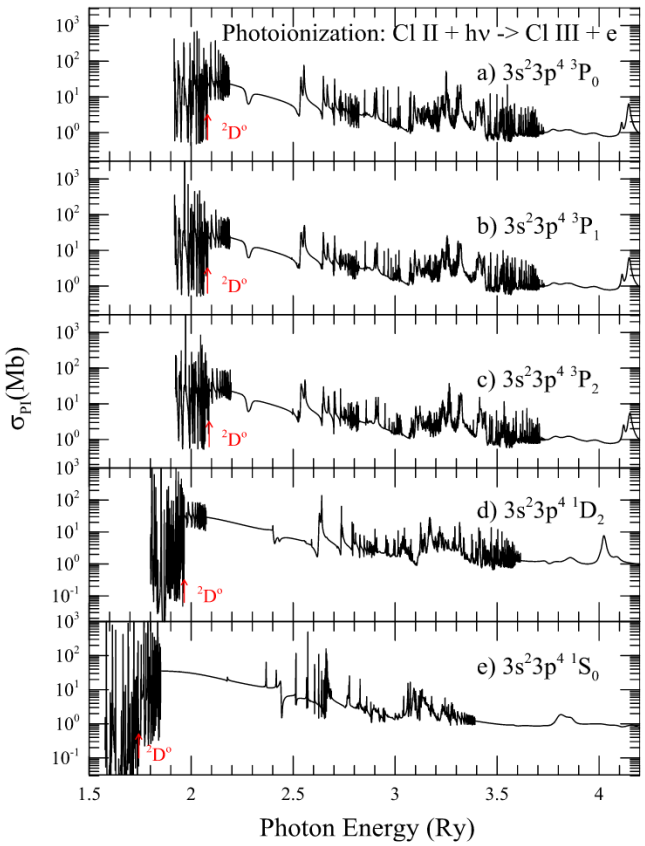

Fig. 1. Photoionization cross sections, σ_{PI}, of the ground $^3P_0$ (a) and four excited, $^3P_{1,2}$, $^1D_2$, $^1S0$ (b-e) levels of the ground configuration $3s^23p^4$ of Cl II. The arrows point to the first excitation threshold of $^2D^o$ state of the core ion Cl III. The region of high peak resonances with almost zero background below the threshold have formed by fine-structure couplings.

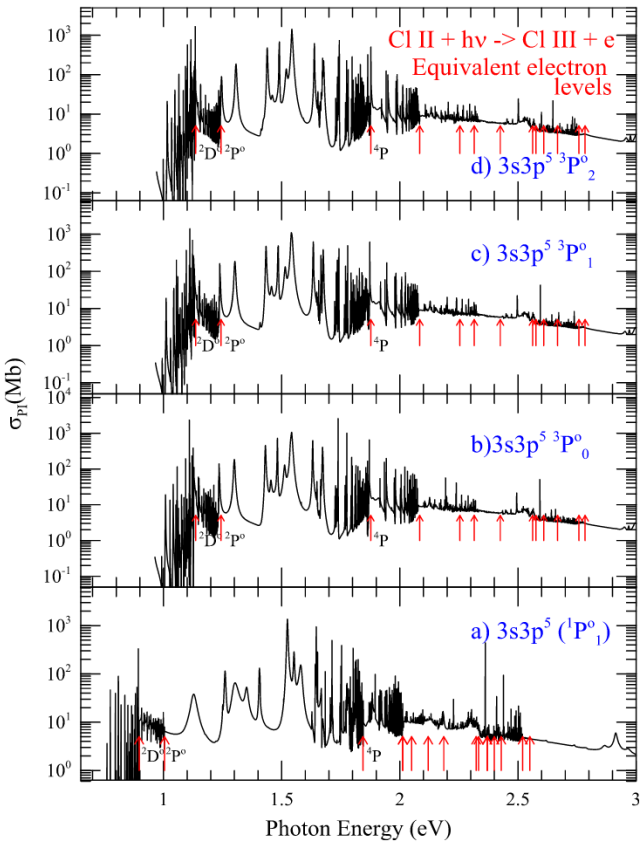

Fig. 2. Photoionization cross sections σ_{PI} of the four excited equivalent electron levels of Cl II: a) $3s\ 3p^5(^1P^o_1)$, b) $3s\ 3p^5(^3P^o_0)$, c) $3s\ 3p^5(^3P^o_1)$, and d) $3s\ 3p^5(^3P^o_2)$. The arrows indicate positions of core ion excitation thresholds. Structures below, ^4P state which is dipole allowed to the ground level $^4S^o$ are more prominent than others.

$3s^23p^3(^2D^o_{3/2,5/2})$ thresholds resulting in the weaker background and stronger resonant peaks. σ_{PI} of each 3 levels of $^3P_{0,1,2}$ and $^1D_2$, $^1S_0$ show this feature. The same feature is seen in photoionization of neutral sulfur, the same electronic structure as of Cl II, which has been studied extensively experimentally (Tondello, 1972; Gibson et al., 2825; Joshi et al., 1987) and theoretically (Tayal, 1988; Altun, 1992). Detail discussion of these resonances is available in these references. These characteristic resonances indicate high rate of ionization at low energy and of the inverse process of electron-ion recombination at low temperature supporting high reactivity of this low charge ion. At higher energies, σ_{PI} of these levels show resonances and a background which is different from a typical smooth decrease in the background of the ground state of an atom or ion. Earlier work by McLaughin (2017) focused only on the energy region of experiment and details on the comparison with experiment and hence does not show the high energy region.

4.3. Photoionization of excited equivalent electron levels

Levels of excited equivalent electron states contribute significantly in the spectral analysis. These levels have more than one electron in the outer orbital. Compared to single valence electron levels, they typically have more compact resonant structures and a background that decreases slow. Fig. 2 illustrates these features for the excited equivalent electron levels of Cl II: a) $3s\ 3p^5(^1P^o_1)$, b) $3s\ 3p^5(^3P^o_0)$, c) $3s\ 3p^5(^3P^o_1)$, and d) $3s\ 3p^5(^3P^o_2)$. Similar to the levels of the ground configuration which are also equivalent electron levels (Fig. 1), these levels show resonant region below the $^2D^o$ thresholds of the core ion (the first arrow in the panels) with near zero background. However the resonances are weaker than those in the rest of energy region. The figure illustrates the impact of various core ion excitations on σ_{PI}. The energy positions of various excitations are pointed by arrows. We see that the most prominent region with enhanced structures is the region below the excited level $3s3p^4(^4P)$. This level is dipole allowed to the ground level $^4S^o$. The high transition probability for the core ion excitation to a dipole allowed level, e.g. $3s^23p^3(^4S^0) - 3s3p^4(^4P)$, enhances photoionization below it (e.g. Nahar, 1998). Beyond this threshold, the structures have become weaker for other excitation thresholds. Two more ^4P states exist in the higher energy region (seen in Table 1). However the resonances below them have weakened indicating convergence of enhancement.

4.4. Benchmarking of photoionization cross sections with experiment

Hernandez et al (2015) who reported the first detailed features of photoionization of Cl II measured the cross section in the energy range of 19.5 - 28.0 eV at a high resolution beam width of 15 meV (Fig. 3, panel a) at the sophisticated set-up of ALS of the synchrotron at LBNL. This energy range corresponds to ionization and features of a number of levels of Cl II. They correspond to the lowest set of levels, such as the 5 levels of the ground configuration, $(3s^23p^4)[^3P_{0,1,2}, ^1D_2, ^1S_0]$, and next excited low lying levels $(3s3p^5)^3P^o_{0,1,2}$, $(3s3p^5)^1P^o_1$, $(3s^23p^33d)^5D^o_{0,1,2,3,4}$, $(3s^23p^34s)^5S^o_2$, and $(3s^23p^34s)^3S^o_1$. All these levels are expected to contribute to the integrated features in the observed spectrum of the experiment. Fig. 3 compares the measured σ_{PI} (panel a) of Cl II with the present theoretical σ_{PI} of the 9 levels (panels b-j) to determine the individual level contributions. The panels b-f present σ_{PI} of the 5 levels of the ground configuration, $(3s^23p^4)[^3P_{0,1,2}, ^1D_2, ^1S_0]$. These are the dominating contributors of the features in the observed spectrum. All

fine structure levels belonging to a LS state show similar structures in σ_{PI}. Hence to compare with the characteristic features of individual states, one level of $(3s3p^5)^3P^o$ and one of $(3s^23p^33d)^5D^o$ have been selected for demonstration. Panels g-j present σ_{PI} of $(3s3p^5)^3P^o_2$, $(3s^23p^33d)^5D^o_2$, $(3s^23p^34s)^5S^o_2$, and $(3s3p^5)^1P^o_1$ respectively. The prominent features in the observed σ_{PI} in panel a have been pointed by arrows which also appear in panels b-j to correlate the theoretical predictions in the 9 lowest levels.

We see that the high resolution resonant lines of panel a match exactly various resonant lines predicted by the 9 levels of Cl II. We note that most of the features at and beyond the ionization threshold of the ground state at about 23.7 eV come from the 3 levels of the ground state ^3P (panels b-d) and below the threshold come from the two other levels $^1D_2$ (panel e) and $^1S_0$ (panel f). The resonance line with the second arrow in panel a matches only those of $(3s3p^5)^3P^o_2$, $(3s^23p^33d)^5D^o_2$, and $(3s^23p^34s)^5S^o_2$. The third observed line matches those of $^1D_2$, $^1S_0$, $^5D^o_2$, $^5S^o_2$, and $^1P^o_1$. There are other observed resonances in panel a) which are seen to be overlapped contributions by more than one level. However, the amount of contributions depend on population of the levels in the experimental beam and other factors. McLaughlin (2017) who studied only the 5 levels of the ground configuration and in the energy range of that of the experimental energy range, missed these resonant contributions from the other levels. The abundances of high lying levels is typically lower as experiments aim at obtaining beam at the ground level. Hence their resonances appear partially and weaker in the observed spectrum. We also see that there are more resonances in theoretical prediction than in the observed cross sections..Ideally all these calculated resonances exist. They belong to the Rydberg series of resonances corresponding to excited levels of the core ion, $S_iL_i(J_i)\pi_i\nu_l\ell$ where $S_iL_i(J_i)\pi_i$ is an excited core ion level and $\nu_l\ell$ are the effect and orbital quantum numbers of a resonance. The effective quantum number ν_l is related to the quantum defect μ_l and principal quantum number n as $\nu = n - \mu$ McLaughlin presents tables of effective quantum numbers and quantum defects of the observed resonant lines. These table values may be useful when used in diagnostics of plasmas. However, for Cl II, the resonance are not well separated and distinct like those of highly charged He- or Li-like ions to be used for diagnostics. Reproducing the features theoretically and identifying them to the specific levels that they belong to have benchmarked both the theoretical and calculated cross sections.

While all resonances can be predicted theoretically, observed lines are only part of them because of the dissolution of resonances by the experimental set-up, such as, the widths of experimental beam and the detector, level populations, and the density of the target. The strength of the observed lines depend on the number of resonances produced by the core ion excitations, abundances of ion levels in the experimental beam. It is possible to reproduce a spectrum similar to the observed integrated features in experimental photoionization cross section by convolving the highly resolved calculated cross sections with a Gaussian function of width equal to that of the photon beam width and then combining the convolved cross sections using assumed population of levels present in the experimental beam (e.g. Nahar, 2002, 2004). To match the experimental shape a fitting procedure is needed since Gaussian function is an approximation but not the exact form of photon distribution function and the abundances of level population in the experimental beam is also not known accurately. Hence the process is not precise. The measured spectrum by Hernandez et al (2015) is highly resolved and does note require any additional processing of data to identify the correspondence between the measured and calculated cross sections and their resonances. For similarity comparison, the present calculated cross sections of Fig. 3 have been convolved with a beam width of 15 meV, as reported in the experiment, and are compared with that of experiment in Fig. 4. Similarities in features are seen clearly in this figure. As in Fig. 3, arrows are pointing to the observed prominent observed features and the correspondence in the theoretical predictions. Although all physical features are matching, slight shift in energy

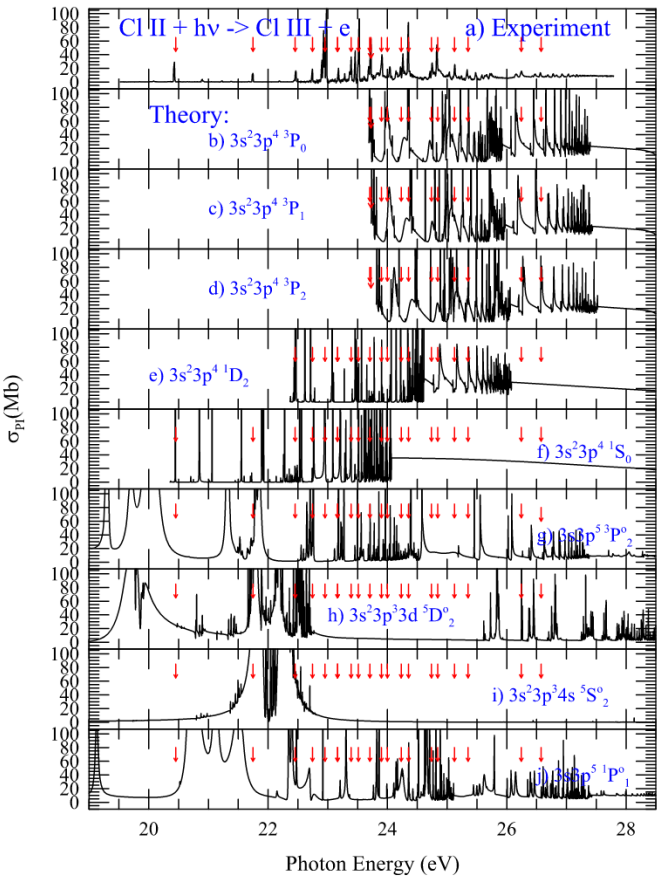

Fig. 3. Comparison of photoionization cross sections σ_{PI} of Cl II between experiment (panel a) by Hernandez et al (2015) and the present theoretical work (panels b-j). The observed features (prominent ones are pointed by arrows in panel a) are reproduced in calculated σ_{PI} of the ground and low lying levels of the ion: $(3s^23p^4)^3P_{0,1,2}$, $^1D_2$, $^1S_0$ (panels b-f), $(3s3p^5)^3P^o_2$ (panel g), $(3s^23p^33d)^5D^o_2$ (panel h), $(3s^23p^34s)^5S^o_2$ (panel i), $(3s3p^5)^1P^o_1$ (panel j).

positions of structures in theoretical σ_{PI} can be noticed; This is due to the slight difference between the calculated and observed energies of excited levels of the core ion.

4.5. Partial cross sections for photoionization in to various core ion levels

Photoionization cross section of a level is the sum of partial cross sections of channels that leave the ion in the ground and various excited levels of the core ion. These partial cross sections are needed for applications, such as, when recombination occurs to the core ion which is left to an excited level after photoionzation in a thin plasma, in study of cascading effects as the excited level drops down etc. Fig. 5 presents features in partial photoionization of the ground level $^3P_0$ of Cl II as the residual ion Cl III is left in 8 lowest levels, the ground $3s^23p^3(^4S^o_{3/2})$ and next seven excited $3s^23p^3(2D^o_{3/2,5/2},^2P^o_{1/2,3/2})$, $3s3p^4(^4P_{1/2,3/2,5/2})$ levels (listed in Table 1). Panel (a) which presents partial σ_{PI} for leaving the core at the ground level $3s^23p^3(^4S^o_{3/2})$ illustrates that the region of narrow resonances at threshold (Fig. 1) of the ground level arise from this channel and the resonances belong to Rydberg series of $3s^23p^3(^2D^o_{5/2})\nu l$ forming $^3S^o_1$,^{3} D^o_1. With higher excited levels of the residual ion, the contributions become weaker.

4.6. Seaton resonances for single valence electron excited levels

One common but prominent feature in photoionization of single valence electron excited levels is the presence of Seaton resonances manifested by photo-excitation-of-core (PEC) from the ground to

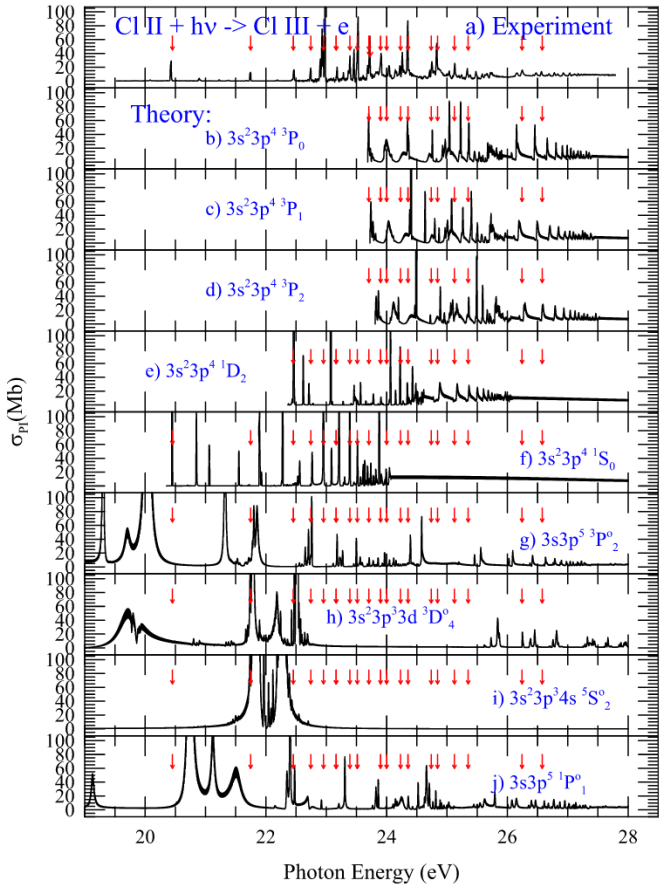

Fig. 4. Comparison of photoionization cross sections σ_{PI} of Cl II between experiment (panel a) by Hernandez et al (2015) and the present theoretical work (panels b-j). The same theoretical cross section of Fig. 3 are presented in the same panels after they have been convolved with a Gaussian function using the experimental beam width of 15 meV. The observed features are pointed by arrows as in Fig. 3. The similarities between the observed and convolved cross sections can be seen easily.

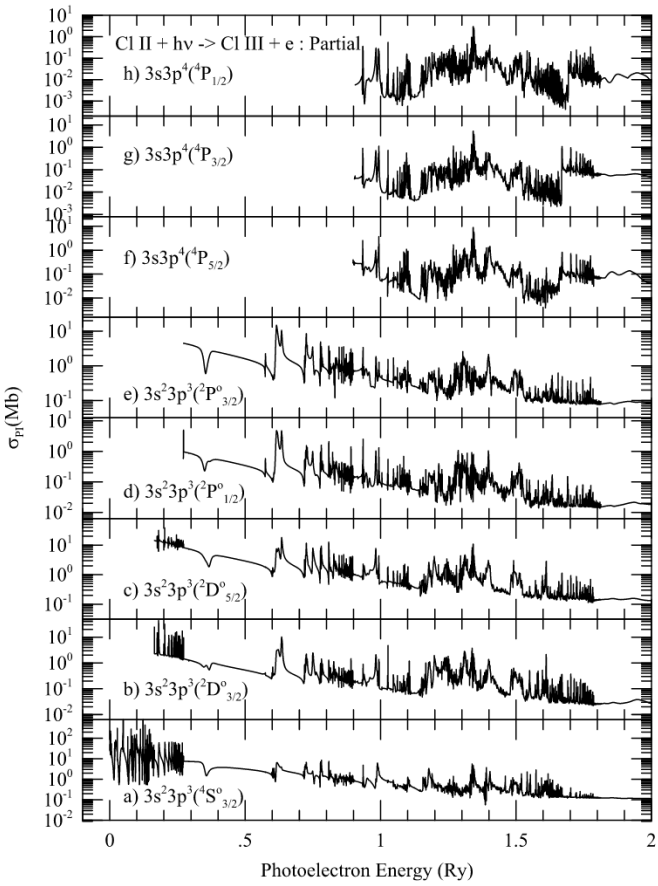

Fig. 5. Partial photoionization cross sections, σ_{PI}, of the ground $^3P_0$ level of Cl II leaving the residual ion Cl III in the ground (a) and next seven excited levels, $3s^23p^3(2D^o_{3/2,5/2},^2\ P^o_{1/2,3/2})$, $3s3p^4(^4P_{1/2,3/2,5/2})$ as specified in panels b-h.

excited dipole allowed levels. These resonances are typically more distinct in higher excited levels than the lower ones, and become narrow at very high excited levels (e.g. Pradhan and Nahar, 2011). The resonance is formed when the core ion absorbs the photon for a dipole allowed transition from the ground level while the outer electron remains as a spectator which is followed by photoionization as the core drops down to the ground level. It was first observed in the study under the Opacity Project and was interpreted by Yu and Seaton (1987). Following Table 1, there are 33 allowed E1 transitions possible from the $3s^23p^3(^4S^o_{3/2})$ ground level of Cl III all of which can introduce the resonances below the excitation threshold energies but at exact transition energies. A Seaton resonance is different from Auger decay where the vacancy of an inner shell is created by ionization which is then filled up by an electron dropping down from an upper level and the energy difference between the two levels, one with the vacancy and one from which the electron is dropping, will cause emission of a photon or ejection of electron from the upper level.

Fig. 6 illustrates Seaton resonances in photoionization of three excited single valence electron levels, (a) $3s^23p^3(^4S^o_{3/2})4s(^3S^o_1)$, (b) $3s^23p^3(^4S^o_{3/2})5p(^3P_1)$, (c) $3s^23p^3(^4S^o_{3/2})4d(^3D^o_1)$. Positions of the Seaton resonances are pointed by arrows. Since the core ion excitations are at fixed transition energies, the resonances appear at the same photon energy positions for all excited levels. Seaton resonances are embedded in and interfere with narrow Rydberg resonances which can result in considerable enhancement in the background cross section. In the figure the dominating high peak Seaton resonances are around 1.64 Ry formed by the dipole allowed excitations from the ground level, $3s^23p^3(^4S^o_{3/2}) - 3s^23p^23d(^4P_{1/2,3/2,5/2})$. The cross sections show huge accumulated impact of interference of Seaton and Rydberg resonances by forming broad features with enhanced background by orders of magnitude in the higher energy region.

Some additional features can be seen beyond the purple arrow in panel (c) of Fig. 6. The purple arrow in each panel indicates the energy position of the highest excited level included in the CC wave function expansion for the R-matrix calculations. This means that all resonances belonging to various core ion excitations up to the highest level in the set are obtained in detail even if the wave function may include more excitations of the core ion. In the present case, the wave function actually contains 283 levels where the first 45 levels have been chosen for the R-matrix calculations. Often the higher terms in the wave function which have not been included in the expansion for the R-matrix computation form broad and low resolution structures beyond the highest excited state, as seen in panel c. They are called as pseudo-resonances as they are not resolved precisely and energy positions also may not be precise. Among the levels beyond these 45 levels for the present case, the energy positions of the next dipole allowed $^4S^o - ^4P$ transitions are at 2.3 Ry, 2.37 Ry, 2.40 Ry and 2.56 Ry respectively as shown by blue arrows in panel (c) of Fig. 6. The structures in the figure appear at these energies and hence correspond to PEC and formation of Seaton resonances.

5. Conclusion

Photoionization cross sections Cl II with a wave function that includes 45 levels of the core ion have been studied for various

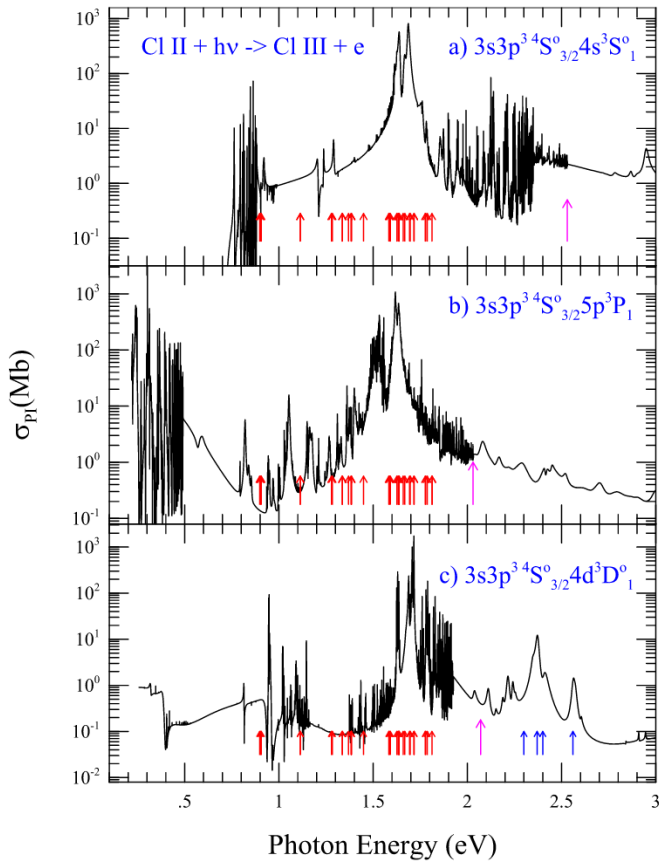

Fig. 6. Photoionization cross sections (σ_{PI}) of three single valence electron excited levels of Cl II, (a) $3s^23p^3(^4S^o_{3/2})4s(^3S^o_1)$, (b) $3s^23p^3(^4S^o_{3/2})5p(^3P_1)$, (c) $3s^23p^3(^4S^o_{3/2})4d(^3D^o_1)$. These illustrate Seaton resonances (pointed by arrows) formed by photo-excitation-of-core (PEC) to dipole allowed levels. The impact of the resonances can be seen in the broad features with enhanced background by orders of magnitude.

characteristic features of equivalent and non-equivalent electron levels. The cross sections have been benchmarked with those measured using the ALS at LBNL. The comparison with experiment has identified the component levels in the experimental beam that produced the resonant features in the experiment. Seaton resonances in σ_{PI} are shown to dominant the high energy region of excited levels. Photoionization cross sections have been obtained for a total number of 392 bound levels of Cl II which should enable complete plasma modelings, such as, of plasma opacities, synthetic spectrum, and diagnostics.

The complete set of data for photoionization cross sections and the energy levels are available on-line from NORAD-Atomic-Data website at: http://norad.astronomy.ohio-state.edu/

CRediT authorship contribution statement

Sultana N. Nahar: Conceptualization, Data curation, Formal analysis, Funding acquisition, Investigation, Methodology, Project administration, Resources, Software, Validation, Visualization, Writing - original draft, Writing - review & editing.

Declaration of Competing Interest

The authors declare that they have no known competing financial interests or personal relationships that could have appeared to influence the work reported in this paper.

Acknowledgment

This work was supported partially by NSF AST-1312441 and AST-1109088. The computational work was carried out at the Ohio Supercomputer Center (OSC) in Columbus Ohio.

Supplementary material

Supplementary material associated with this article can be found, in the online version, at 10.1016/j.newast.2020.101447 .

References

Altun, Z., 1992. J. Phys. B 25, 2279.
Berrington, K.A., Burke, P.G., Butler, K., Seaton, M.J., Storey, P.J., Taylor, K.T., Yu, Y., 1987. Atomic data for opacity calculations. II. Computational methods. J. Phys. B 20, 6379–6397.
Berrington, K.A., Eissner, W., Norrington, P.H., 1995. RMATRIX1 belfast atomic R-matrix codes. Comput. Phys. Commun 92, 290–420.
Burke, P.G., Robb, W.D., 1975. R-matrix theory of atomic processes. Adv. Atom. Mol. Phys. 11, 143–214.
Dufour, R.J., 1984. APJ 287, 341–352.
Eissner, W., Jones, M., Nussbaumer, H., 1974. Techniques for the calculation of atomic structures and radiative data including relativistic corrections. Comput. Phys. Commun. 8, 270–306.
Energies, N. W. f. t. o. c. ,. Http //physics.nist.gov/cgi-bin/AtData/main_asd.
Fegley Jr., B., Zolotov, M.Y., 2000. Icarus 148 (1), 193–210.
Hernandex, E.M., 2015. JQSRT 151, 217–223.
Hummer, D. G., Berrington, K. A., Eissner, W., Pradhan, A. K., Saraph, H. E., Tully, J. A.,. Atomic data from the IRON Project. 1 Goals and methodsAstron. Astrophys. 1003 (279), 298–309.
Martin, W. C., Kaufman, W., Sugar, J., Musgrove, A.,. Preliminary compilation of wavelengths and energy-levels for the spectra of chlorine. (1992–1997) unpublished, available at NIST website.
McLaughin, B.M., 2017. MNRAS 464, 1990–1999.
Joshi, Y.N., Mazzoni, M., Nencioni, A., Parkinson, W.H., Cantu, A., 1987. J. Phys. B 20, 1203.
Nahar, S.N., 1998. Pra 58, 3755.
Nahar, S.N., 2002. Phys. Rev. A 65, 052702.
Nahar, S.N., 2004. Phys. Rev. A 69, 042714.
Nahar, S.N., 2014. Oscillator strengths and transition probabilities fromthe breit paulir-matrix method neIV. Atom. Data Nucl. Data Tables 100, 1322–1336.
Nahar, S.N., Eissner, W., Chen, G.X., Pradhan, A.K., 2003. Atomic data from the iron project - LIII. Relativistic allowed and forbidden transition probabilities for fe XVII. A&A 408, 789–801.
Nahar, S.N., Pradhan, A.K., 1994. Unified treatment of electron-ion recombination in the close-coupling approximation. Phys. Rev. A 49, 1816–1835.
Nahar, S.N., Pradhan, A.K., 2000. Large-scale breit-pauli R-matrix calculations for transition probabilities of Fe V. Phys. Scr. 61, 675–689.
Pradhan, A.K., Nahar, S.N., 2011. Atomic Astrophysics and Spectroscopy. Cambridge University press.
Radziemski Jr., L.J., Kaufman, V., 1974. J. Opt. Soc. Am. 64, 366–389.
Seaton, M.J., 1987. J. Phys. B 20, 6363–6378.
Gibson, S.T., Greene, J.P., Rusek, B., Berkowitz, J., 1986. J. Phys. B 19.
Tayal, S.S., 1988. Phys. Rev. A 38, 729–736.
Team, T.O.P., 1996. The Opacity Project, Vol 1, 1995, Vol. 2. Institute of Physics Publishing.
Tondello, G., 1972. Astrophys. J 172, 771.
Website, N.,. Http //norad.astronomy.ohio-state.edu.
Yu, Y., Seaton, M.J., 1987. Atomic data for opacity calculations. IV. Photoionisation cross sections for C II. J. Phys. B 20, 6409–6429.
Zhang, H.L., Nahar, S.N., Pradhan, A.K., 1999. Close coupling r-matrix calculations for electron-ion recombination cross sections. J. Phys. B 32, 1459–1479.